Hidden Area and Mechanical Nonlinearities in Freestanding Graphene

Ryan J. T. Nicholl,[1] Nickolay V. Lavrik,[2] Ivan Vlassiouk,[3] Bernadeta R. Srijanto,[2] and Kirill I. Bolotin[1,4,*]
[1]Department of Physics and Astronomy, Vanderbilt University, Nashville, Tennessee 37235, USA
[2]Center for Nanophase Materials Sciences, Oak Ridge National Laboratory, Oak Ridge, Tennessee 37831, USA
[3]Energy and Transportation Science Division, Oak Ridge National Laboratory, Oak Ridge, Tennessee 37831, USA
[4]Department of Physics, Freie Universität Berlin, Arnimallee 14, Berlin 14195, Germany
(Received 8 February 2017; published 27 June 2017)

We investigated the effect of out-of-plane crumpling on the mechanical response of graphene membranes. In our experiments, stress was applied to graphene membranes using pressurized gas while the strain state was monitored through two complementary techniques: interferometric profilometry and Raman spectroscopy. By comparing the data obtained through these two techniques, we determined the geometric hidden area which quantifies the crumpling strength. While the devices with hidden area ∼0% obeyed linear mechanics with biaxial stiffness 428 ± 10 N/m, specimens with hidden area in the range 0.5%–1.0% were found to obey an anomalous nonlinear Hooke's law with an exponent ∼0.1.

DOI: 10.1103/PhysRevLett.118.266101

A thin membrane is always crumpled due to its low bending rigidity and resulting inability to sustain compressive forces. Such crumpling has been actively investigated during the last three decades to describe the behaviors of wrinkled skin [1,2], biological lipid membranes [3,4], and solar sails [5]. The advent of graphene and other 2D materials allowed for testing the models of crumpling in crystalline membranes at the ultimate atomic thickness limit [6]. In graphene specifically, crumpling originates from static wrinkling [7–9] and out-of-plane (flexural) phonons [10–12] and persists in both supported and freestanding samples [13]. Recent theoretical work showed that every mechanical property of graphene is renormalized due to crumpling [14–20]. In particular, crumpling causes the reduction of the stiffness [21,22], increased bending rigidity [11,23], variable (and negative) Poisson's ratio [24,25], and negative thermal expansion [26,27]. At the same time, the contribution due to crumpling is almost universally ignored in the experiments probing mechanics of these materials. This may lead to misinterpretation or incorrect conclusions, for example, while using graphene nanoelectromechanical devices to detect mass, force, or displacement. Experiments that do probe the interplay between crumpling and graphene mechanics remain highly challenging [21,23,28].

Previously, we developed an approach to probe the mechanical response of crumpled graphene membranes [29]. We observed the reduction of graphene stiffness down to ∼20 N/m and hypothesized that it was mostly due to static wrinkling. Unfortunately, the electrostatic actuation scheme used in that work prevented us from applying sufficient stress to change the crumpling strength. Because of that, while the hints of nonlinear behavior in stress-strain curves were observed, we could not investigate it in detail.

The goal of this Letter was to study the transition of graphene membranes from the crumpled state characterized by reduced stiffness to the flat state with accepted stiffness close to 400 N/m (Young's modulus ∼1 TPa). To apply mechanical stress sufficient to drive this transition, some membranes were pressurized with compressed gas while others were prestressed during fabrication. To characterize the transition, we quantified the degree of crumpling by comparing the measurements of strain via Raman spectroscopy and wide-field interferometry. These experimental innovations allowed the observation of a nonlinear Hooke's law in samples with different amounts of crumpling. Our findings were confirmed by the comparison with quantitative theory.

Experimental setup.—Two types of samples were produced: standard and strain engineered. Both sample types were prepared by the wet transfer of graphene grown via chemical vapor deposition with subsequent thermal annealing as described in a previous work [29]. Standard samples consisted of a monolayer graphene membrane suspended over a single hole with diameter ∼10 μm in a silicon nitride (SiN_x) support on a silicon chip [Fig. 1(a), left]. To create strain-engineered samples, we patterned an additional ∼50–100 nm–deep, 5-μm-wide recess in the SiN_x around the edges of the hole [Fig. 1(a), right]. Graphene was pulled into the recess by van der Waals forces during transfer. From geometrical considerations, this process is expected to impart ≤1% strain on graphene. Strain-engineered samples allow us to extend the range of applicable stress and act as an experimental control for flat graphene subjected to perfectly in-plane and uniform built-in stress.

The mechanical response of graphene membranes was characterized through measurements of sample deflection under a known pressure (P). Pressure was applied to graphene using compressed nitrogen gas [30] as shown in Fig. 1(b) and the Supplemental Material (SM) [31]. From pressure, we determined the radial stress [33] of graphene $\sigma = Pa^2/4h$, where h is the center point displacement determined from interferometry described below and $a \sim 5$ μm is the radius of the device. We note that σ is

 © 2017 American Physical Society

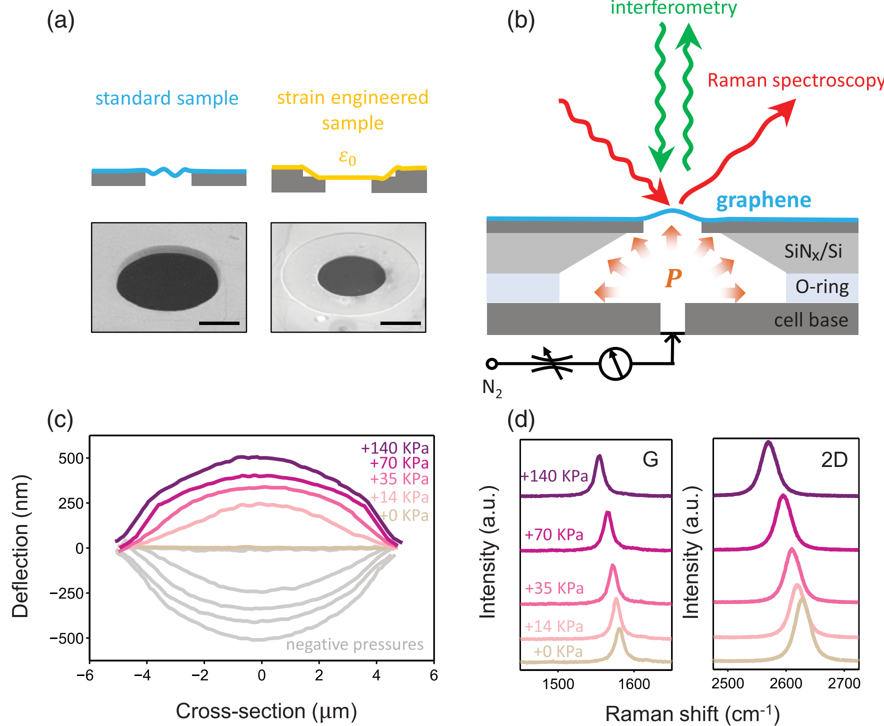

FIG. 1. Experimental setup. (a) Top row: Cartoon views of standard and strain-engineered devices. Bottom row: scanning electron microscopy images of representative samples (scale bar is 5 μm). (b) Device schematic showing the application of pressure and our two measurement techniques, interferometry and Raman spectroscopy. Depending on the orientation of the sample chip we can apply positive (away from the sample, as pictured) or negative (towards the sample) pressures. (c) Membrane profiles for both positive and negative pressures as measured by wide-field interferometry. (d) Raman spectra of graphene showing the G and 2D Raman peaks throughout the range of applied pressure.

the total stress that includes both the built-in (existing without the application of pressure) and applied (due to applied pressure) stress components. Consequently, $\sigma = 0$ means the membrane is completely relaxed.

Upon application of pressure, the mechanical strain ε of the graphene membrane was measured in two different yet complementary approaches: interferometric profilometry ($\varepsilon_{\mathrm{Int}}$) and Raman spectroscopy ($\varepsilon_{\mathrm{Ram}}$). The strain ε determined by both measurement types is applied strain. By definition, $\varepsilon = 0$ at zero applied pressure. In the first method, the deflection of graphene is probed via wide-field phase shift interferometry using a 530-nm, <0.1 mW power illumination. This allowed the direct determination of lateral membrane topography on the micron scale [Fig. 1(c)] and the measurement of the center point deflection (h) with nanometer resolution. From geometrical considerations, the radial strain [33] was then determined as $\varepsilon_{\mathrm{Int}} = 2h^2/3a^2$. Because $\varepsilon_{\mathrm{Int}}$ is measured geometrically relative to the initial state at $P = 0$, it does not include the built-in strain (ε_0) component.

In our second method, the strain was determined by monitoring the shifts of the 2D and G peaks in the Raman spectra of graphene taken at the center of the membrane. Inaccuracy of spot position by up to 2 μm changes the results no more than 4%, see SM Fig. 2 [31]. We use a focused 633-nm excitation source with an estimated spot size <1 μm, resolution ~ 1 cm^{-1} and power <1 mW to

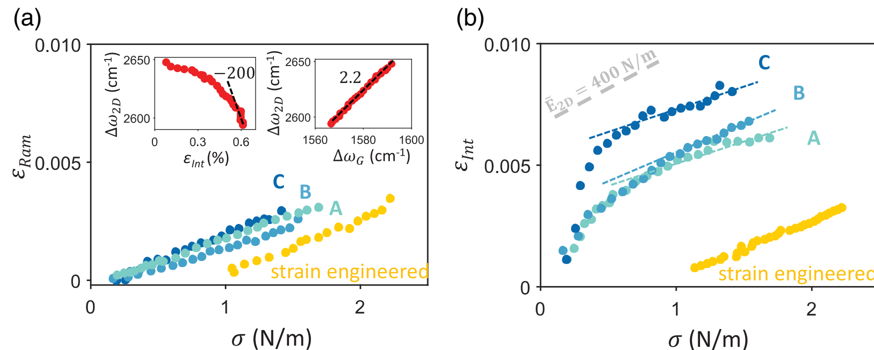

FIG. 2. Stress-strain curves from interferometry and Raman spectroscopy. (a) Stress-strain as determined from Raman spectroscopy, $\varepsilon_{\mathrm{Ram}}(\sigma)$, for three standard samples A, B, and C (blue points) along with a strain engineered device (orange points). The data for the strain-engineered device is offset for clarity. Left inset: The progression of Raman 2D peak shift vs $\varepsilon_{\mathrm{Int}}$ used to calibrate peak sensitivity $\partial\omega/\partial\varepsilon$ (dashed black line). Right inset: The position of the 2D Raman peak plotted vs the position of the G Raman peak. The slope of 2.2 indicates that changes in peak positions are due to strain. (b) Stress-strain as determined from interferometry, $\varepsilon_{\mathrm{Int}}(\sigma)$, for the same devices shown in (a). Dashed grey line shows slope expected for flat graphene with the stiffness $\tilde{E}_{2D} = 400$ N/m. Dashed colored lines indicate the region of linear mechanical behavior.

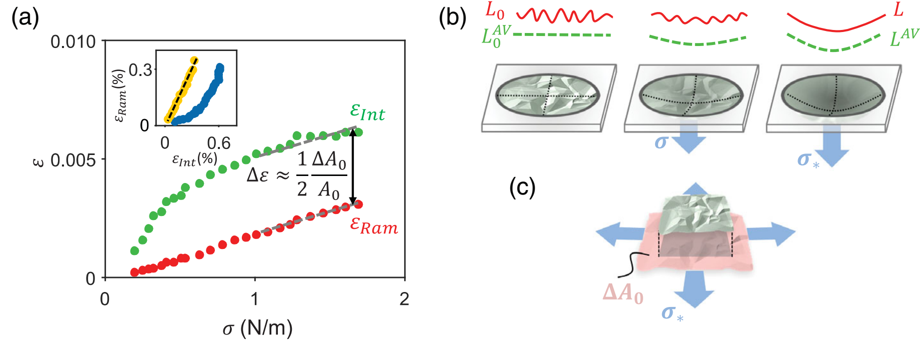

FIG. 3. The relation between strain and crumpling. (a) The comparison of the strain measured via interferometry ($\varepsilon_{\rm Int}$, green curve) and the strain determined via Raman spectroscopy ($\varepsilon_{\rm Ram}$, red curve) vs applied stress σ for device A. Inset: $\varepsilon_{\rm Ram}$ vs $\varepsilon_{\rm Int}$ for the same device shown in the main panel (blue points) and strain-engineered device (orange points). Dashed black line has slope $\sim$1. (b) Cartoon illustrating the evolution of crumpling in a membrane under gradually increasing stress. Cross section of the membrane and the same cross section averaged with micron resolution are shown above each membrane. (c) Visualization of hidden area ΔA_0 of a membrane.

avoid heating [Fig. 1(d)]. The strain was extracted as $\varepsilon_{\rm Ram}^{\rm 2D,G} = (\partial\omega^{\rm 2D,G}/\partial\varepsilon_{\rm Ram}^{\rm 2D,G})^{-1}(\omega^{\rm 2D,G} - \omega_0^{\rm 2D,G})$ [34]. Here $\omega^{2D,G}$ is the frequency position of the 2D(G) peak of strained graphene and $\omega_0^{\rm 2D,G}$ is the position of the same peak at zero applied pressure. In this way, $\varepsilon_{\rm Ram}$ is also a measurement of strain relative to the initial state [35]. The peak sensitivity for each device was found by extracting the slope of Raman peak positions vs $\varepsilon_{\rm Int}$ [Fig. 2(a), left inset, dashed line] at stresses >1 N/m. We find peak sensitivities $|\partial\omega^{\rm 2D}/\partial\varepsilon_{\rm Int}| \sim 155$–$200\ {\rm cm}^{-1}/\%$ and $|\partial\omega^{G}/\partial\varepsilon_{\rm Int}| \sim 55 - 90\ {\rm cm}^{-1}/\%$ consistent with recent values in literature [34,36–38]. The necessity of applying such large stress is discussed later. We ensured that changes in Raman peak positions vs pressure were entirely due to strain rather than, e.g., changes in doping by observing $\partial\omega^{\rm 2D}/\partial\omega^{G} \sim 2.2$ [Fig. 2(b), right inset] [39]. This also confirms identical results for extraction of strain from either G or 2D peaks.

Comparison of stress-strain curves from interferometry and Raman spectroscopy.—The stress-strain relationships of three standard samples (A, B, and C) as measured from Raman spectroscopy, $\varepsilon_{\rm Ram}(\sigma)$, and interferometry, $\varepsilon_{\rm Int}(\sigma)$, are shown in Figs. 2(a) and 2(b). We observe dramatic differences between the $\varepsilon_{\rm Ram}(\sigma)$ and $\varepsilon_{\rm Int}(\sigma)$ curves. The $\varepsilon_{\rm Ram}(\sigma)$ curves are linear [Fig. 2(a)]. The average biaxial modulus for all devices extracted from them is $\tilde{E}_{\rm 2D} = d\sigma/d\varepsilon_{\rm Ram} = 480 \pm 10$ N/m. In contrast, the $\varepsilon_{\rm Int}(\sigma)$ curves are strongly nonlinear [Fig. 2(b)]. In the region of low stress ($\sigma < 1$ N/m), graphene is soft, $\tilde{E}_{\rm 2D} \sim 30$–$150$ N/m. At the same time, in the high-stress region ($\sigma > 1$ N/m) we retrieve an average value of $\tilde{E}_{\rm 2D} = 450 \pm 70$ N/m, close to what is measured by Raman spectroscopy. In the most interesting intermediate region ($\sigma \sim 1$ N/m), we see a transition from nonlinear to linear mechanical response with increasing stress. For the strain-engineered device [Figs. 2(a) and 2(b), orange points], we observe a linear and identical response from both Raman spectroscopy ($\tilde{E}_{\rm 2D} = 430 \pm 10$ N/m) and interferometry ($\tilde{E}_{\rm 2D} = 426 \pm 7$ N/m) throughout the range of applied stress.

We note that the biaxial moduli measured from Raman spectroscopy or from interferometry at high stress are close to the values obtained in other experiments [40–42], consistent with the value for flat graphene, $\tilde{E}_{\rm 2D} \sim 400$ N/m calculated from Lamé parameters [27] ($\lambda = 2$ eV Å^{-2} and $\mu = 10$ eV Å^{-2}) and extracted from simulations [43]. The biaxial modulus can be converted to an in-plane stiffness, $E_{\rm 2D} = (1-\upsilon)\tilde{E}_{\rm 2D}$, where $\upsilon \sim 0.165$ is the commonly used value for the Poisson's ratio of graphene [44]. This yields an average of $E_{\rm 2D} = 380 \pm 30$ N/m over all our devices. This corresponds to a Young's modulus of $\sim$1 TPa. However, the Poisson's ratio for graphene is not well known and may not be constant or may even take negative values [24,25]. Therefore, we directly report the biaxial modulus $\tilde{E}_{\rm 2D}$.

The data of Fig. 2 invite the following questions. Why are the observed behavior and magnitudes of $\varepsilon_{\rm Ram}$ and $\varepsilon_{\rm Int}$ so different? What is the nature of the nonlinearity in $\varepsilon_{\rm Int}$ and can we quantify it?

The relation between stress-strain curves and crumpling.—We believe the disparity between $\varepsilon_{\rm Ram}(\sigma)$ and $\varepsilon_{\rm Int}(\sigma)$ is a signature of crumpling and can be understood by clarifying the definition of strain. The shifts of Raman peaks, and hence $\varepsilon_{\rm Ram}(\sigma)$ derived from them, reflect length changes of the carbon-carbon (C—C) bonds. Quantitatively, $\varepsilon_{\rm Ram} = (L - L_0)/L_0$, where L_0 and L are the lengths of the membrane before and after the application of stress. The "true" length of the membrane L is not affected by crumpling provided C—C bond lengths are unchanged [45]. On the other hand, interferometric profilometry senses the profile of the membrane averaged with micrometer resolution, $\varepsilon_{\rm Int} = (L^{\rm AV} - L_0^{\rm AV})/L_0^{\rm AV}$, where $L_0^{\rm AV}$ and $L^{\rm AV}$ are the lengths of the *averaged* profiles. Thus defined $L^{\rm AV}$ decreases when the membrane is crumpled. The difference between L (red lines) and $L^{\rm AV}$ (dashed green lines) is illustrated in the cartoon of Fig. 3(b) showing cross sections of circular membranes under the application of stress. At zero applied stress, crumpling causes a large difference between the "true" length of the cross section, L_0, and the length of its averaged profile, $L_0^{\rm AV}$. When the stress is large enough to

suppress crumpling (σ_*), that difference vanishes and the true profile is virtually indistinguishable from the averaged profile, $L \sim L^{AV}$. Summarizing, ε_{Ram} is the microscopic strain, which is a relative change in the bond lengths or the change in true membrane length, whereas ε_{Int} is macroscopic strain, which is a relative change in the length of the averaged profile.

This insight allows the following interpretation of the data. At small stress, the changes in L^{AV} per unit stress are large compared to those in L as the significant amount of "hidden" length contained in crumpling is being unraveled [Fig. 3(b), middle]. In the experimental data at $\sigma < \sigma_* \sim 1$ N/m, we indeed observe much larger $d\varepsilon_{Int}/d\sigma$ compared to $d\varepsilon_{Ram}/d\sigma$ [Fig. 3(a)]. As the stress becomes larger, the amount of crumpling is gradually decreased. Finally, the crumpling is suppressed, the membrane is flat, and the difference between the change in L and L^{AV} disappears almost completely [Fig. 3(b), right]. Correspondingly, in standard devices at $\sigma > \sigma_* \sim 1$ N/m [Fig. 3(a)] or in strain-engineered devices [Fig. 3(a), inset, orange points] we observe $d\varepsilon_{Int}/d\sigma \sim d\varepsilon_{Ram}/d\sigma$ or, equivalently, $d\varepsilon_{Ram}/d\varepsilon_{Int} \sim 1$.

The near-constant difference $\Delta\varepsilon = \varepsilon_{Int}(\sigma) - \varepsilon_{Ram}(\sigma)$ observed in the regime of high stress is related to what is known as "hidden area" in geometry [22]. The hidden area ΔA_0 is the difference between the true area of the membrane A_0 and the A_0^{AV} area of its projection onto a plane parallel to the membrane at zero applied stress [46]. As is evident from Fig. 3(c), ΔA_0 is the amount of area "hidden" in out-of-plane crumpling and is "revealed" when the membrane is stretched. From simple geometrical considerations, $\Delta\varepsilon \approx (L_0^{AV} - L_0)/L_0 \approx \frac{1}{2}(A_0^{AV} - A_0)/A_0 = \frac{1}{2}\Delta A_0/A_0$. We use the relative hidden area $\Delta A_0/A_0$ extracted from $\Delta\varepsilon$ to quantify the amount of crumpling in our devices. We obtain relatively large $\Delta A_0/A_0$ of 0.6%, 0.8%, and 1.0% for devices A, B, and C, respectively.

Exploring the nonlinear response.—Having obtained a quantitative measure for crumpling strength, we further investigate the nonlinear behavior of the macroscopic strain (ε_{Int}) relevant for most experiments. Recently, a theory [47] was developed to describe the "anomalous Hooke's law" in the stress-strain relationship of crumpled graphene,

$$\varepsilon(\sigma) = \frac{\sigma_*}{\tilde{E}_{2D}}\left[\frac{\sigma}{\sigma_*} + \frac{1}{\alpha}\left(\frac{\sigma}{\sigma_*}\right)^{\alpha}\right]. \quad (1)$$

Here, α is an exponent which determines the degree of nonlinearity caused by crumpling and σ_* is the "crossover stress," a measure of the stress required to flatten the membrane. Qualitatively, the mechanical behavior described by Eq. (1) is that of two springs in series. The first linear "spring," with stiffness $\tilde{E}_{2D} \sim 400$ N/m, describes the stretching of C—C bonds, while the second, nonlinear "spring" corresponds to the uncrumpling of a membrane. The theory of Ref. [47] predicts $\alpha \sim 0.1$ for static disorder (wrinkling) and $\alpha \sim 0.5$ for thermal fluctuations (flexural phonons).

The comparison of our experimental data with the predictions of Eq. (1) is greatly facilitated by our complementary measurements of ε_{Int} and ε_{Ram}. By taking the difference $\varepsilon_{Int}(\sigma) - \varepsilon_{Ram}(\sigma)$, we isolate the contribution of the nonlinear term in Eq. (1) pertaining to the mechanics of crumpling. To account for built-in stress in our devices, we subtract an additional term $\varepsilon_0 = \varepsilon(\sigma_0)$ from Eq. (1), where σ_0 is built-in stress. This allows us to compare our data (where only applied strain is measured) with Eq. (1). We are then able to fit our experimental data for devices A, B, and C to the nonlinear component in Eq. (1) with $\tilde{E}_{2D}$ determined from interferometry at high stress with α, σ_*, and σ_0 treated as free parameters.

Figure 4(a) illustrates the adherence of our data to the nonlinear model. For all standard devices, we retrieve an average exponent $\alpha = 0.12 \pm 0.02$. This is close to $\alpha = 0.1$ expected for statically wrinkled graphene, confirming our earlier interpretation that static wrinkling rather than flexural phonons is the primary contributor to crumpling [29]. The average value of built-in stress obtained from the fit, $\sigma_0 = 0.07 \pm 0.01$ N/m, is close to what is observed by others [42,48]. The average crossover stress was found to be $\sigma_* = 0.8 \pm 0.1$ N/m. Physically, this means a stress of at least 0.8 N/m was required to flatten the sample and retrieve a linear response at higher stress. In agreement with that, linear $\varepsilon(\sigma)$ was observed for the strain-engineered device where we estimate $\sigma_0 = 0.84 \pm 0.02$ N/m ($>\sigma_*$). Possible reasons for deviations from the model include nonuniform stress fields, nonrandom wrinkle distribution, deviation of the geometry from perfectly circular, and possible presence of contaminants [49,50].

The notion of the hidden area can be further used to compare the data to the prediction of the model of Ref. [47]. There, the degree of crumpling was controlled by the "disorder parameter," $B \propto (\sigma_* - \sigma_0)/\tilde{E}_{2D}$. In Fig. 4(b),

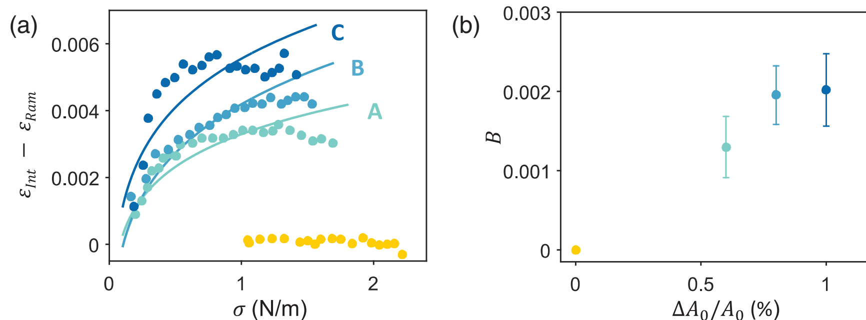

FIG. 4. Nonlinear mechanics in crumpled graphene. (a) The difference between the strain extracted from interferometry and the strain from Raman $\varepsilon_{Int} - \varepsilon_{Ram}$ vs stress σ for standard samples A, B, and C (blue points) and the strain-engineered device (orange points). Solid lines are fits to the nonlinear model described in the main text ($\varepsilon \propto \sigma^{\alpha}$). (b) Disorder parameter B vs hidden area $\Delta A_0/A_0$.

parameter B extracted from our fits vs $\Delta A_0/A_0$ is plotted. The correlation seen in Fig. 4(b) means that higher crumpling measured experimentally does, in fact, correspond to higher disorder in the model.

Conclusion.—In conclusion, we observed the crossover from nonlinear mechanical response of graphene in the regime of low applied stress described by an anomalous Hooke's law, to linear response at high stress. The degree of nonlinearity and the crossover stress were found to depend on the amount of crumpling. We determined the latter, as quantified by the hidden area, through complementary Raman spectroscopy and interferometry measurements. Furthermore, we have demonstrated the distinction between experimentally measuring the microscopic or macroscopic mechanical response of materials.

We would like to highlight a few possible applications of our results. First, in many nanomechanics experiments, the linear mechanical response of graphene and other 2D materials is assumed in the regime of low stress (e.g., Refs. [51,52]). The conclusions of some of these works may need to be reassessed. Second, our results suggest that the mechanical constants of graphene can be engineered in a wide range by tailoring the amount of crumpling through strain engineering. Finally, the most exciting area for future work is at the intersection between condensed-matter and statistical physics, where it may be possible to study renormalization of elastic constants of crystalline membranes due to flexural phonons [53,54] and the competition between crumpling sources [16].

We acknowledge enlightening conversations with I. V. Gornyi, V. Y. Kachorovskii, and A. D. Mirlin as well as financial support from Defense Threat Reduction Agency Basic Research Grant No. HDTRA1-15-1-0036, NSF Grant No. CAREER 4-20-632-3391, the Sloan Foundation, and ERC Grant No. 639739. The optical profilometry measurements and fabrication of the chips for graphene transfer were conducted at the Center for Nanophase Materials Sciences, which is a DOE Office of Science User Facility.

[*]Corresponding author.
kirill.bolotin@fu-berlin.de

[1] E. Cerda and L. Mahadevan, Phys. Rev. Lett. **90**, 074302 (2003).
[2] J. Genzer and J. Groenewold, Soft Matter **2**, 310 (2006).
[3] W. Helfrich and R.-M. Servuss, Nuovo Cimento Soc. Ital. Fis. **3**, 137 (1984).
[4] E. Evans and W. Rawicz, Phys. Rev. Lett. **64**, 2094 (1990).
[5] W. Wong and S. Pellegrino, J. Mech. Mater. Struct. **1**, 3 (2006).
[6] H. Vandeparre, M. Piñeirua, F. Brau, B. Roman, J. Bico, C. Gay, W. Bao, C. N. Lau, P. M. Reis, and P. Damman, Phys. Rev. Lett. **106**, 224301 (2011).
[7] N. Liu, Z. Pan, L. Fu, C. Zhang, B. Dai, and Z. Liu, Nano Res. **4**, 996 (2011).
[8] S. Deng and V. Berry, Mater. Today (Oxford, U. K.) **19**, 197 (2016).
[9] W. Bao, F. Miao, Z. Chen, H. Zhang, W. Jang, C. Dames, and C. N. Lau, Nat. Nanotechnol. **4**, 562 (2009).
[10] A. Fasolino, J. H. Los, and M. I. Katsnelson, Nat. Mater. **6**, 858 (2007).
[11] R. Ramírez, E. Chacón, and C. P. Herrero, Phys. Rev. B **93**, 235419 (2016).
[12] J. C. Meyer, A. K. Geim, M. I. Katsnelson, K. S. Novoselov, T. J. Booth, and S. Roth, Nature (London) **446**, 60 (2007).
[13] D. A. Kirilenko, A. T. Dideykin, and G. Van Tendeloo, Phys. Rev. B **84**, 235417 (2011).
[14] A. Košmrlj and D. R. Nelson, Phys. Rev. E **89**, 0022126 (2014).
[15] A. Košmrlj and D. R. Nelson, Phys. Rev. B **93**, 125431 (2016).
[16] I. V. Gornyi, V. Y. Kachorovskii, and A. D. Mirlin, Phys. Rev. B **92**, 155428 (2015).
[17] J. H. Los, A. Fasolino, and M. I. Katsnelson, Phys. Rev. Lett. **116**, 015901 (2016).
[18] M. J. Bowick, A. Kosmrlj, D. R. Nelson, and R. Sknepnek, Phys. Rev. B **95**, 104109 (2017).
[19] D. Wan, D. R. Nelson, and M. J. Bowick, arXiv:1702.01863.
[20] J. H. Los, A. Fasolino, and M. I. Katsnelson, arXiv:1703.08400.
[21] C. S. Ruiz-Vargas, H. L. Zhuang, P. Y. Huang, A. M. van der Zande, S. Garg, P. L. McEuen, D. A. Muller, R. G. Hennig, and J. Park, Nano Lett. **11**, 2259 (2011).
[22] A. Košmrlj and D. R. Nelson, Phys. Rev. E **88**, 012136 (2013).
[23] M. K. Blees, A. W. Barnard, P. A. Rose, S. P. Roberts, K. L. McGill, P. Y. Huang, A. R. Ruyack, J. W. Kevek, B. Kobrin, D. A. Muller, and P. L. McEuen, Nature (London) **524**, 204 (2015).
[24] J.-W. Jiang, T. Chang, X. Guo, and H. S. Park, Nano Lett. **16**, 5286 (2016).
[25] J.-W. Jiang and H. S. Park, Nano Lett. **16**, 2657 (2016).
[26] D. Yoon, Y.-W. Son, and H. Cheong, Nano Lett. **11**, 3227 (2011).
[27] P. L. de Andres, F. Guinea, and M. I. Katsnelson, Phys. Rev. B **86**, 144103 (2012).
[28] G. López-Polín, C. Gómez-Navarro, V. Parente, F. Guinea, M. I. Katsnelson, F. Pérez-Murano, and J. Gómez-Herrero, Nat. Phys. **11**, 26 (2015).
[29] R. J. T. Nicholl, H. J. Conley, N. V. Lavrik, I. Vlassiouk, Y. S. Puzyrev, V. P. Sreenivas, S. T. Pantelides, and K. I. Bolotin, Nat. Commun. **6**, 8789 (2015).
[30] S. P. Koenig, N. G. Boddeti, M. L. Dunn, and J. S. Bunch, Nat. Nanotechnol. **6**, 543 (2011).
[31] See Supplemental Material at http://link.aps.org/supplemental/10.1103/PhysRevLett.118.266101 for additional data, which includes Ref. [32].
[32] N. G. Boddeti, S. P. Koenig, R. Long, J. Xiao, J. S. Bunch, and M. L. Dunn, J. Appl. Mech. **80**, 040909 (2013).
[33] M. K. Small and W. D. Nix, J. Mater. Res. **7**, 1553 (1992).
[34] T. M. G. Mohiuddin, A. Lombardo, R. R. Nair, A. Bonetti, G. Savini, R. Jalil, N. Bonini, D. M. Basko, C. Galiotis, N. Marzari, K. S. Novoselov, A. K. Geim, and A. C. Ferrari, Phys. Rev. B **79**, 205433 (2009).
[35] While built-in strain can be estimated from the Raman spectra, we cannot separate strain-induced shifts from those caused by doping from contaminants. Neglecting that doping, we estimate a compressive built-in strain between 0.01% and 0.09%.

[36] C. Metzger, S. Rémi, M. Liu, S. V. Kusminskiy, A. H. Castro Neto, A. K. Swan, and B. B. Goldberg, Nano Lett. **10**, 6 (2010).
[37] C. Androulidakis, E. N. Koukaras, J. Parthenios, G. Kalosakas, K. Papagelis, and C. Galiotis, Sci. Rep. **5**, 18219 (2015).
[38] D. Metten, F. Federspiel, M. Romeo, and S. Berciaud, Phys. Rev. Applied **2**, 054008 (2014).
[39] J. E. Lee, G. Ahn, J. Shim, Y. S. Lee, and S. Ryu, Nat. Commun. **3**, 1024 (2012).
[40] T. J. Booth, P. Blake, R. R. Nair, D. Jiang, E. W. Hill, U. Bangert, A. Bleloch, M. Gass, K. S. Novoselov, M. I. Katsnelson, and A. K. Geim, Nano Lett. **8**, 2442 (2008).
[41] J. S. Bunch, S. S. Verbridge, J. S. Alden, A. M. van der Zande, J. M. Parpia, H. G. Craighead, and P. L. McEuen, Nano Lett. **8**, 2458 (2008).
[42] C. Lee, X. Wei, J. W. Kysar, and J. Hone, Science **321**, 385 (2008).
[43] W. Gao and R. Huang, J. Mech. Phys. Solids **66**, 42 (2014).
[44] O. L. Blakslee, D. G. Proctor, E. J. Seldin, G. B. Spence, and T. Weng, J. Appl. Phys. **41**, 3373 (1970).
[45] We observe that Raman spectra for our standard samples are similar to that of substrate-supported samples and that changes in the spectra vs stress are similar in standard and strain-engineered samples. From that, we conclude that the amount of crumpling in our experiment is not sufficient to affect the C—C bonds.
[46] R. Ramírez and C. P. Herrero, Phys. Rev. B **95**, 045423 (2017).
[47] I. V. Gornyi, V. Y. Kachorovskii, and A. D. Mirlin, 2D Mater. **4**, 011003 (2017).
[48] I. W. Frank, D. M. Tanenbaum, A. M. van der Zande, and P. L. McEuen, J. Vac. Sci. Technol. B **25**, 2558 (2007).
[49] C. Berger, M. Dirschka, and A. Vijayaraghavan, Nanoscale **8**, 17928 (2016).
[50] We recognize that there may be polymeric residues left on our devices from the fabrication stage. While such residues may contribute to crumpling, their direct effect on the mechanical response of the membrane is expected to be insignificant [49].
[51] W. Bao, K. Myhro, Z. Zhao, Z. Chen, W. Jang, L. Jing, F. Miao, H. Zhang, C. Dames, and C. N. Lau, Nano Lett. **12**, 5470 (2012).
[52] C. Chen, S. Rosenblatt, K. I. Bolotin, W. Kalb, P. Kim, I. Kymissis, H. L. Stormer, T. F. Heinz, and J. Hone, Nat. Nanotechnol. **4**, 861 (2009).
[53] D. R. Nelson and L. Peliti, J. Phys. **48**, 1085 (1987).
[54] J. A. Aronovitz and T. C. Lubensky, Phys. Rev. Lett. **60**, 2634 (1988).